Cell Reports

Article

PD-1$^+$ Tcf1$^+$ CD8$^+$ T cells from established chronic infection can form memory while retaining a stableimprint of persistent antigen exposure

Graphical abstract

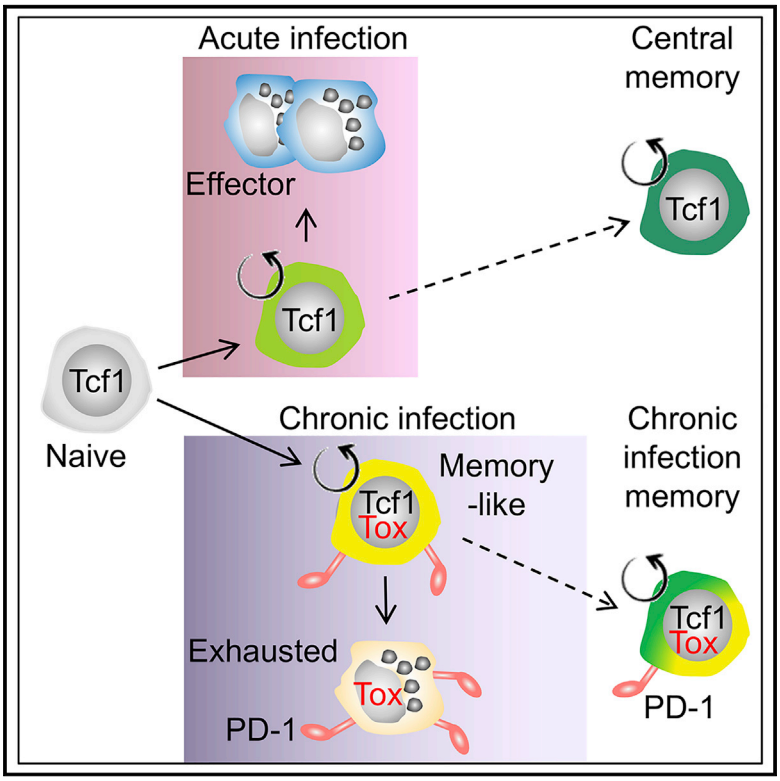

Authors

Mélanie Charmoy, Tania Wyss, Mauro Delorenzi, Werner Held

Correspondence

werner.held@unil.ch

In brief

Although memory-like PD-1$^+$ Tcf1$^+$ CD8$^+$ T cells (T_{ML}s) sustain the immune response to chronic viral infection, the fate of these cells in the absence of persistent stimulation has remained unclear. Charmoy et al. find that T_{ML}s can yield functional memory that retains a permanent imprint of prior chronic stimulation.

Highlights

- PD-1$^+$ Tcf1$^+$ CD8$^+$ T cells (T_{ML}s) establish memory upon clearance of chronic infection
- T_{ML}-derived memory cells globally resemble conventional memory CD8$^+$ T cells
- T_{ML}-derived memory cells retain a permanent imprint of prior chronic stimulation
- Persistent Tox expression explains the chronic infection imprint in memory cells

Charmoy et al., 2021, Cell Reports *36*, 109672
September 7, 2021 © 2021 The Author(s).
https://doi.org/10.1016/j.celrep.2021.109672

CellPress

Cell Reports

CellPress
OPEN ACCESS

Article

PD-1$^+$ Tcf1$^+$ CD8$^+$ T cells from established chronic infection can form memory while retaining a stable imprint of persistent antigen exposure

Mélanie Charmoy,[1] Tania Wyss,[2] Mauro Delorenzi,[1,2] and Werner Held[1,3,*]
[1]Department of Oncology, University of Lausanne, Lausanne, Switzerland
[2]SIB Swiss Institute of Bioinformatics, Bioinformatics Core Facility, Lausanne, Switzerland
[3]Lead contact
*Correspondence: werner.held@unil.ch
https://doi.org/10.1016/j.celrep.2021.109672

SUMMARY

Virus-specific PD1$^+$ Tcf1$^+$ memory-like CD8$^+$ T cells (T_{ML}s) maintain the CD8$^+$ T cell response during chronic viral infection. However, the fate of these cells following cessation of persistent antigen exposure has been unclear. Here, we find that T_{ML}s persist upon transfer into antigen-free hosts and form memory following recall stimulation. Phenotypic, functional, and transcriptome analyses show that T_{ML}-derived memory cells resemble those arising in response to acute, resolved infection, but they retain features of chronically stimulated cells, including elevated PD-1 and Tox and reduced cytokine expression. This chronic infection imprint is largely accounted for by constitutive Tox expression. Virus-specific Tcf1$^+$ CD8$^+$ T cells that persist after clearance of systemic infection also display a chronic infection imprint. Notwithstanding, renewed virus exposure induces a recall response, which controls virus infection in part. Thus, cessation of chronic antigen exposure yields a memory CD8$^+$ T cell compartment that reflects prior stimulation.

INTRODUCTION

Persistent exposure to antigens during chronic viral infection promotes the terminal differentiation of virus-specific CD8$^+$ T cells. This is associated with limited effector functions and the upregulation of negative regulators of T cell function, such as the co-inhibitory receptors PD-1 (programmed cell death protein 1 (*Pdcd1*) and LAG3 (Wherry and Kurachi, 2015). The production of terminally differentiated cells in chronic infection is sustained by a subset of virus-specific CD8$^+$ T cells that is identified by, and depends on, the expression of T cell factor 1 (Tcf1, encoded by the *Tcf7* gene). In addition, these cells are characterized by Ly108 (Slamf6) and CXCR5 expression in combination with inhibitory receptors, including PD-1 and LAG3 (Utzschneider et al., 2016; Im et al., 2016; Wu et al., 2016). Because Tcf1$^+$ PD-1$^+$ CD8$^+$ T cells persist in the presence of antigens, they are referred to as memory-like CD8$^+$ T cells (T_{ML}s) or, alternatively, as progenitor exhausted cells (Blank et al., 2019).

Functionally, T_{ML}s have recall expansion and self-renewal capacity, and they continuously generate differentiated Tcf1$^-$ PD-1$^+$ CD8$^+$ T cells (referred to as terminally exhausted CD8$^+$ T cells [T_{EX}s]) that have cytolytic potential. T_{EX}s express additional inhibitory receptors, such as Tim3. Furthermore, recent data show that T_{EX}s are heterogeneous, whereby CX3CR1$^+$ cells have cytolytic potential and are necessary to keep virus infection under control (Hudson et al., 2019; Zander et al., 2019).

The clearance of acute infection results in the formation of memory, i.e., the persistence of pathogen-experienced cells in the absence of the antigen. The memory CD8$^+$ T cell compartment includes central memory cells (T_{CM}s) that have potent recall expansion, self-renewal, and differentiation capacity. These cells maintain the immune response through repeated episodes of pathogen exposures. Effector memory cells (T_{EM}s) have reduced recall expansion capacity but exert readily available cytotoxic activity and can, thus, provide more immediate protection from reinfection (Kaech and Cui, 2012). T_{CM}s have classically been distinguished from T_{EM}s by the expression of CD62L (Sallusto et al., 1999). We recently reported that *Tcf7* expression refines that discrimination because both CD62L$^+$ *Tcf7*$^+$ and CD62L$^-$ *Tcf7*$^+$ memory cells have T_{CM} properties, whereas *Tcf7*$^-$ memory cells correspond to T_{EM}s (Pais Ferreira et al., 2020).

CD8$^+$ T cells responding to chronic infection display distinct transcriptional programs and an altered use of transcription factors compared with conventional effector and memory cells (Doering et al., 2012). For example, the transcription factor Tox is only transiently expressed by CD8$^+$ T cells during acute infections but is continuously expressed during chronic infection, where it contributes to the altered phenotype and reduced function of virus-specific CD8$^+$ T cells (Alfei et al., 2019; Khan et al., 2019; Scott et al., 2019; Yao et al., 2019). Analyses of CD8$^+$ T cell subsets using bulk RNA sequencing (RNA-seq) analyses have further shown that T_{ML}s are transcriptionally distinct from conventional memory subsets (Utzschneider et al., 2016). However, it is not known to what extent those differences are stable or reflect a distinct activation status that depends on antigen

This is an open access article under the CC BY-NC-ND license (http://creativecommons.org/licenses/by-nc-nd/4.0/).

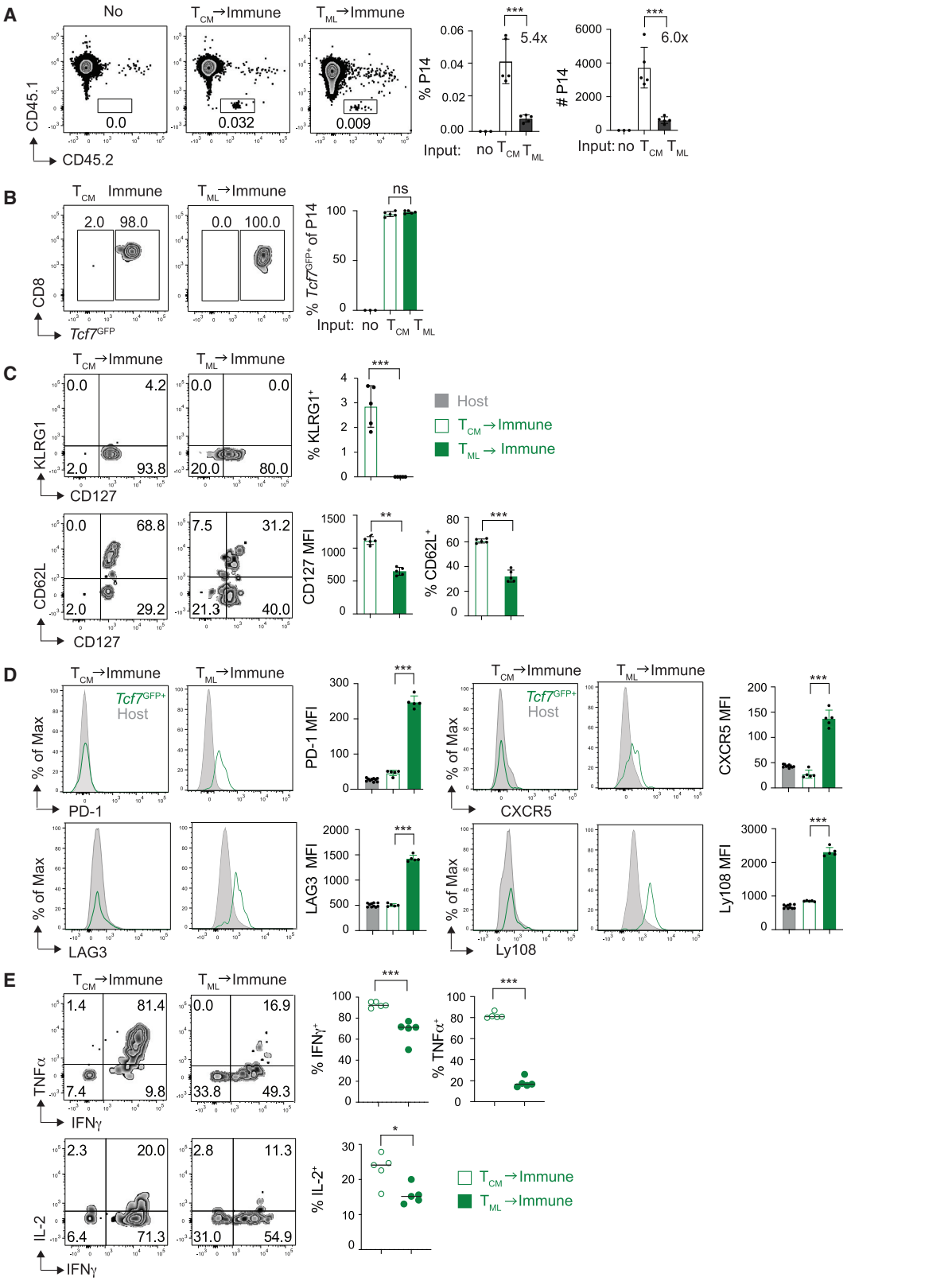

(legend on next page)

persistence. Moreover, the functional capacities of T_{ML} and T_{CM} have not been systematically compared. For example, it was not clear whether T_{ML}s can form memory, i.e., persist in the absence of antigen.

Even though immune-competent mice eventually control viremia associated with chronic lymphocytic choriomeningitis virus (LCMV) clone 13 (cl13) infection, based on the production of neutralizing antibodies (Bergthaler et al., 2009), infectious virus is present indefinitely in certain tissues (Wherry et al., 2003). Thus, antigen remains present long-term in these mice. However, virus-specific $CD8^+$ T cells did not persist upon transfer into antigen-free mice (Shin et al., 2007), some cells were detected upon transfer in antigen-free LCMV-immune recipients (Angelosanto et al., 2012). However, it was not clear whether such memory cells derived from chronically stimulated cells or whether they were recruited into the response at a late stage.

Here, we have used adoptive transfers to address the fate of T_{ML}s, excluding potential confounding effects of thymus-derived T cells. We find that T_{ML}s can persist after antigen withdrawal and yield memory in response to recall. Even though the T_{ML}-derived memory cells resemble conventional memory cells, they keep a phenotypic, transcriptional, and functional imprint of the persistent antigen stimulation. Virus-specific $Tcf1^+$ $CD8^+$ T cells that persist after the clearance of systemic infection displayed similar features. Nevertheless, they significantly protected against renewed virus challenge. These findings showed that cessation of chronic-antigen stimulation yielded a memory $CD8^+$ T cell compartment that mirrored the initial response.

RESULTS

PD-1^+ $Tcf1^+$ $CD8^+$ T cells persist and maintain a chronic infection phenotype in antigen-free hosts

To address whether PD-1^+ $Tcf1^+$ $CD8^+$ T cells (T_{ML}s) from established chronic viral infections can form memory, we determined whether those cells were maintained in the absence of the antigen. To generate T_{ML}s, naive LCMV gp33 epitope-specific $CD8^+$ T cell (P14 cells) (CD45.2) expressing a $Tcf7^{GFP}$ reporter were transferred into Vβ5 transgenic mice (CD45.1). These recipients were then infected with LCMV clone 13 (hereafter, referred to as cl13), which causes chronic viral infection. T_{ML}s are distinguished from T_{EX}s by the expression of $Tcf7^{GFP}$ (Utzschneider et al., 2016) (Figure S1). For functional comparisons, we also generated T_{CM}s. Naive P14 cells were transferred into C57BL/6 (B6) recipients that were infected with LCMV Armstrong (referred to as Arm), which causes acute, resolved viral infection. In mice that have cleared Arm infection (Arm-immune), $Tcf7^{GFP}$ expression identifies T_{CM}s and distinguishes them from T_{EM}s (Pais Ferreira et al., 2020) (Figure S1).

To address their maintenance in the absence of antigens, we transferred flow-sorted T_{ML}s or T_{CM}s into recipient mice that were immune to a LCMV strain with a mutated gp33 epitope (Δgp33) (Johnson et al., 2015). LCMV Δgp33 immune mice were used to bypass potential problems of virus transfer from cl13-infected donor mice, which could initiate an additional round of infection and to ensure the absence of cognate antigens in the recipient mice to prevent restimulation of transferred P14 cells. Three weeks after adoptive transfer, T_{ML}-derived cells were readily detected in the spleen of immune-recipient mice, although their abundance was reduced 6-fold compared with that of the transfer of T_{CM}s (Figure 1A). Similar to T_{CM}s, transferred T_{ML}s retained $Tcf7^{GFP}$ expression (Figure 1B). Thus, unlike T_{ML}s transferred into chronically infected recipient mice (Utzschneider et al., 2016), we did not observe differentiated $Tcf7^-$ cells, suggesting that T_{ML} differentiation was driven by antigen/chronic infection. In addition, the transferred T_{ML}s maintained their $CD62L^+$ or $KLRG1^-$ phenotype but gained CD127 expression compared with the input cells (Figures 1C and S1B). Further, T_{ML}s maintained a chronic infection phenotype, characterized by elevated levels of PD-1, LAG3, CXCR5, and Ly108 and reduced interferon γ (IFN-γ), tumor necrosis factor α (TNF-α), and interleukin 2 (IL-2) production compared with transferred T_{CM}s, although the differences were reduced compared with that of the input cells (Figures 1D, 1E, and S1C–S1E). Thus, T_{ML} persisted in the absence of antigens and maintained a chronic infection phenotype, suggesting a stable cell state.

We further determined whether the reduced abundance of transferred T_{ML}s was related to a reduced ability of T_{ML}s to engraft in recipient mice. Indeed, compared with T_{CM}s, T_{ML}s had a 2.8-fold reduced capacity to engraft the spleen of naive recipients (Figure S2A). We further used intravenous staining with anti-CD8α monoclonal antibody (mAb) to determine the localization of the transferred cells in the spleen. The fraction of stained T_{ML}s that is considered perivascular was not different from that of T_{CM}s (Figure S2B). Together, these data indicated that the spleen homing properties of T_{ML}s were qualitatively similar, albeit reduced, compared with that of T_{CM}s. The latter explained to a significant extent the reduced abundance of T_{ML}s upon antigen withdrawal.

T_{ML}-like cells persist after recall stimulation

We next addressed the fate of T_{ML}s after recall stimulation. Flow-sorted T_{CM}s or T_{ML}s were transferred into naive B6 mice that were then infected with LCMV Arm (referred to as T_{CM}→Arm and T_{ML}→Arm, respectively), and the recall response was

Figure 1. PD-1^+ $Tcf1^+$ $CD8^+$ T cells persist and maintain a chronic infection phenotype in antigen-free hosts

(A–D) B6 mice (CD45.1) that were immune to LCMV Δgp33 (d 21 p.i.) (Immune) were transferred with d 34 p.i. T_{ML}s (T_{ML}→immune) or T_{CM}s (T_{CM}→immune) (CD45.2) or no cells. Recipient mice were analyzed 3 weeks later for the presence of transferred P14 cells (A). The numbers in the bar graphs depict the mean fold difference between T_{CM}→immune and T_{ML}→immune P14 cells. P14 cells were then analyzed for the expression of $Tcf7^{GFP}$ (B); the differentiation markers KLRG1, CD127, and CD62L (C); and the exhaustion markers PD-1 and LAG3 and the T_{ML} markers CXCR5 and Ly108 (D).

(E) Splenocytes were restimulated with gp33 peptide *in vitro*, and P14 cells were analyzed for the production of IFN-γ, TNF-α, and IL-2. Bar and dot graphs show the percentage of positive cells, the abundance of cells, or the mean fluorescence intensity (MFI) of staining.

Data are representative of two experiments each, with n = 3–5 mice per group. All error bars are SD. Statistics are based on unpaired two-tailed Student's t test, whereby significance is indicated as *$p < 0.05$, **$p < 0.01$, ***$p < 0.001$; and ns (not significantly different; $p > 0.05$).

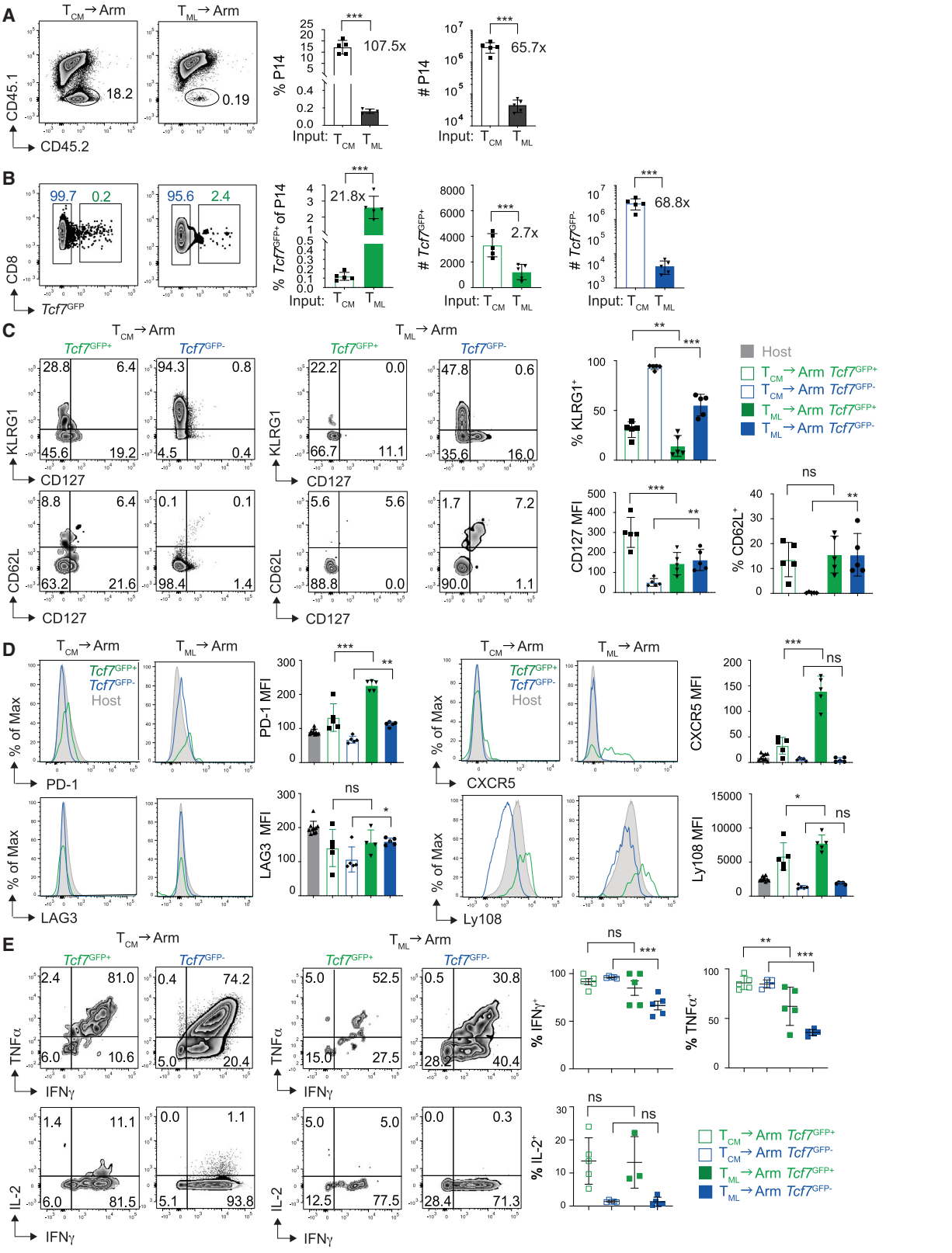

(legend on next page)

analyzed on day 8 post infection (d 8 p.i.). Although the recall expansion of T_{CM}s was 3,000-fold, that of T_{ML}s was only 46-fold (reduced 65.7-fold) (Figure 2A). However, T_{ML}-derived *Tcf7*$^{GFP+}$ was only 2.7-fold reduced (Figure 2B). Considering the reduced engraftment (2.8-fold) (Figure S2A), T_{ML}s seemed to reproduce as efficiently as T_{CM}s. On the other hand, T_{ML}s yield very few differentiated *Tcf7*$^{GFP-}$ cells (reduced 68.8-fold) (Figure 2B), and the residual *Tcf7*$^{GFP-}$ cells were less differentiated, as judged by reduced KLRG1 and increased CD127 and CD62L expression compared with T_{CM}-derived *Tcf7*$^{-}$ cells (Figure 2C). Thus, T_{ML}s seemed to efficiently reproduce but were severely impaired in their ability to generate differentiated cells. The latter correlated with reduced expression of the cell-cycle marker Ki67 by T_{ML}-derived cells, whereby the reduction of cycling Ki67^{+} DAPI^{+} cells was particularly prominent among T_{ML}-derived Tcf1^{+} cells (Figure S3A). In addition, preliminary experiments showed that T_{ML}-derived *Tcf7*$^{GFP-}$ cells were more prone to undergo apoptosis (Figure S3B).

T_{ML}-derived cells *Tcf7*$^{GFP-}$ cells maintained a chronic infection phenotype characterized by increased PD-1 and LAG3 expression and reduced IFN-γ and TNF-α production compared with the corresponding T_{CM} derived cells (Figures 2D and 2E), consistent with a prior analysis of unfractionated, virus-specific CD8^{+} T cells (Utzschneider et al., 2013). T_{ML}-derived *Tcf7*$^{GFP+}$ cells also showed increased PD-1, Ly108, and CXCR5 and decreased TNF-α expression, but LAG3, IFN-γ, and IL-2 were not different from T_{CM}-derived *Tcf7*$^{GFP+}$ cells (Figures 2D and 2E). Thus, acute re-stimulation of T_{ML}s yielded few differentiated *Tcf7*$^{-}$ effector cells, which maintained a chronic infection phenotype and a near-normal number of *Tcf7*$^{+}$ cells with a reduced chronic-infection phenotype.

T_{ML}s yield a memory compartment with an imprint of prior chronic stimulation

We further addressed the capacity of T_{ML}s and T_{CM}s to form a memory in response to acute, resolved infection. At d 50 after LCMV Arm infection, T_{ML}-derived cells had yielded a sizable memory compartment (Figure 3A) although it was reduced 9.5-fold compared with that of T_{CM}-derived memory cells (Figure 3A). T_{ML}-derived *Tcf7*$^{GFP+}$ memory cells were only 2.7-fold reduced (Figure 3B), which corresponded to the reduced initial engraftment (Figure S2A). This indicated that T_{ML}s produced *Tcf7*$^{+}$ memory cells as efficiently as T_{CM}s do. Although *Tcf7*$^{GFP+}$ memory cells comparably expressed CD62L, CD127, and KLRG1 (Figure S4A), T_{ML}-derived *Tcf7*$^{GFP+}$ memory cells retained hallmarks of prior chronic antigen exposure, including increased expression of PD-1, LAG3, CXCR5, Ly108, and Tox and reduced production of TNF-α and IL-2 (Figures 3C–3E). On the other hand, T_{ML}s yielded few *Tcf7*$^{GFP-}$ memory cells (reduced 19.1-fold) (Figure 3B), and these were less differentiated (Figure S4A) but retained increased LAG3 and Tox and reduced IFN-γ, TNF-α, and IL-2 expression compared with T_{CM}-derived *Tcf7*$^{GFP-}$ memory cells (Figures 3C–3E).

We further addressed the recall response of T_{ML}-derived *Tcf7*$^{+}$ memory cells using tertiary transfers. T_{CM}- and T_{ML}-derived *Tcf7*$^{+}$ memory cells expanded comparably and yielded similar numbers of differentiated *Tcf7*$^{-}$ progeny (Figures 3F and 3G). Both types of memory cells also yielded *Tcf7*$^{GFP+}$ progeny, which had expanded compared with that of the input and were even more abundant when they were originally derived from T_{ML}s (Figure 3G). These data showed that T_{ML}s retained self-renewal capacity. The T_{ML}-derived tertiary cells had a less-differentiated phenotype (increased CD127 and reduced KLRG1) yet retained, in part, a chronic-infection phenotype (increased PD-1, CXCR5, and Tox) compared with that of the corresponding T_{CM}-derived cells (Figures S4B and S4C). Thus, memory formation had corrected the expansion/differentiation defect of T_{ML}s, but the cells stably maintained features of the initial exposure to chronic infection during at least two episodes of acute restimulation.

scRNA-seq analysis of the T_{ML}-derived memory cells

To address the basis for the chronic infection imprint, we compared the transcriptomes of memory cells deriving from T_{CM}s (T_{CM}→Arm) to that of memory cells deriving from T_{ML}s (T_{ML}→Arm) by single-cell RNA-seq (scRNA-seq) (Figure S5A). The analysis further included Arm-immune CD8^{+} T cells (Arm), CD8^{+} T cells responding to cl13 infection (cl13), and naive CD8^{+} T cells (naive).

Unsupervised clustering of the five types of P14 cells, using a shared nearest neighbor (SNN) modularity optimization-based clustering algorithm, identified eight discrete clusters of P14 cells (Figure 4A). Cluster 7 (C7) and C8 contained <100 cells and were not analyzed further. Splenic P14 cells responding to Arm or cl13 infection were partitioned into separate areas, distinct from the naive P14 cells (Figure 4B), and each part of two main clusters of cells (Figure 4C; Table S1). We next determined the correspondence of the main cell clusters to known CD8^{+} T cell subtypes using previously established bulk RNA-seq-based gene signatures that derived from naive CD8^{+} T cells (T_{N}s), T_{ML}s, T_{EX}s, T_{CM}s, and T_{EM}s (Utzschneider et al., 2016). The transcriptome of Arm-immune C4 cells (Figure 4C) correlated best with the T_{CM} signature (Figure 4D), as exemplified by the high expression of *Tcf7* and *Il7r* (CD127) and low expression of *Klrg1*, *GzmB*, and *Cx3cr1* (Figure S5B). Arm-immune C1 cells, which were characterized by high *Klrg1* and

Figure 2. T_{ML}-like cells persist after recall stimulation

(A–D) T_{CM} (Arm *Tcf7*$^{GFP+}$) and T_{ML} (cl13 *Tcf7*$^{GFP+}$) P14 cells (CD45.2^{+}) were flow sorted on d 42 p.i. and transferred into B6 recipients (CD45.1/2), which were then infected with LCMV Arm. Abundance (A) and expression of *Tcf7*^{GFP} (B) by T_{CM}→Arm and T_{ML}→Arm memory cells at d 8 p.i. The numbers in the bar graphs depict the mean fold difference between T_{CM}→Arm and T_{ML}→Arm P14 cells. *Tcf7*$^{GFP+}$ and *Tcf7*$^{GFP-}$ P14 cells were analyzed separately for the expression of the differentiation markers KLRG1, CD127, and CD62L (C) and the exhaustion/T_{ML} markers PD-1, LAG-3, Ly108, and CXCR5 (D).

(E) Splenocytes were restimulated with gp33 peptide *in vitro*, and P14 cells were analyzed for the production of IFN-γ, TNF-α, and IL-2.

Data in (A)–(E) are representative of two experiments with n = 3–5 mice per group. All error bars are SD. Statistics are based on unpaired two-tailed Student's t test (A and B) or on ANOVA with Fisher test (C–E), whereby the significance between the indicated groups is shown as *p < 0.05, **p < 0.01, ***p < 0.001; and ns (p > 0.05).

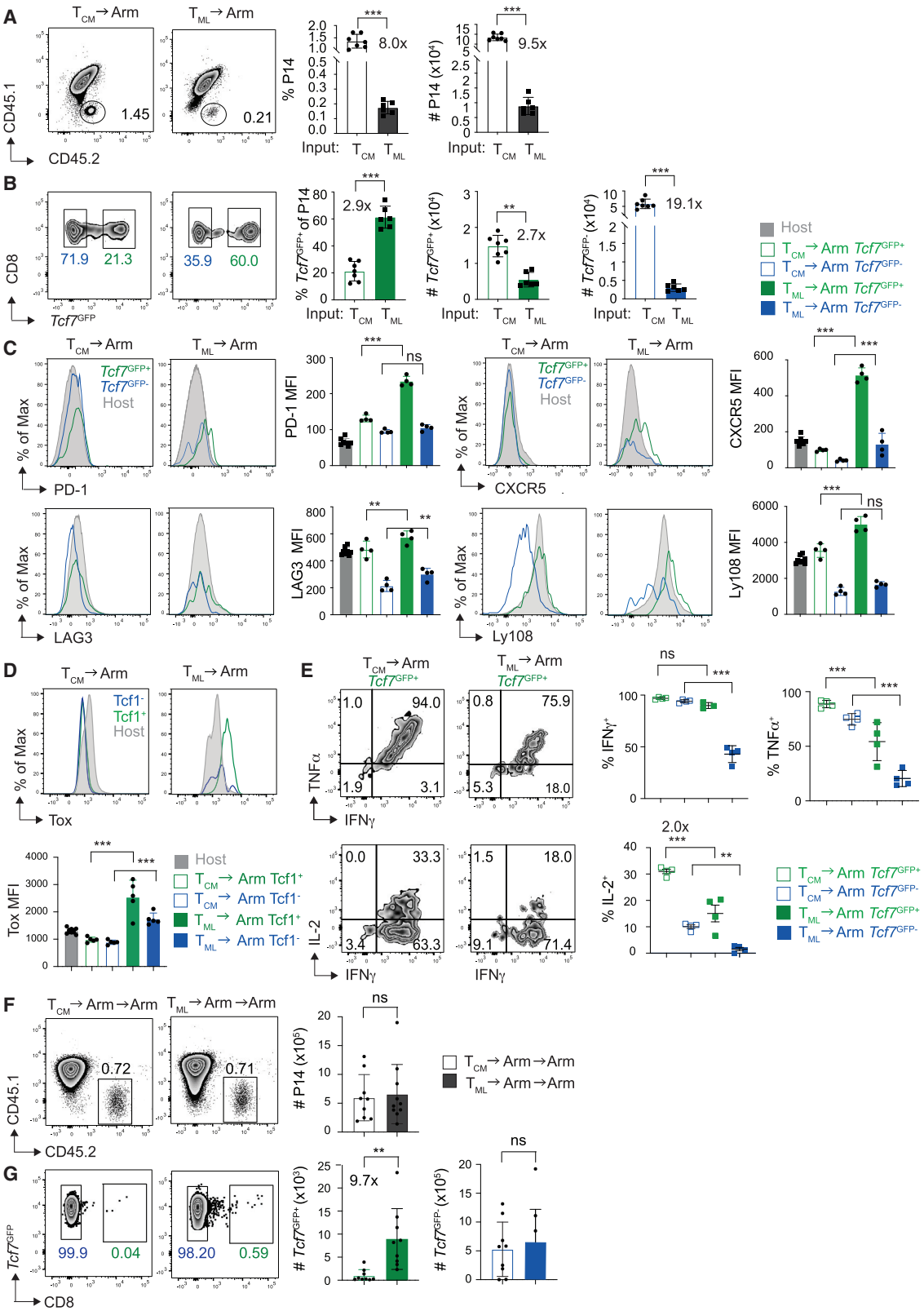

(legend on next page)

Cx3cr1 and intermediate *Tcf7, Il7r*, and *GzmB* expression (Figure S5B), had the greatest correlation with the T_{EM} signature (Figure 4D).

Secondary T_{CM}→Arm memory cells overlapped with primary-Arm memory cells and were part of C4 and C1 (Figure 4E; Table S1). Like Arm C1 cells, the transcriptome of T_{CM}→Arm C1 cells correlated best with the T_{EM} signature but had lost its similarity with the T_{CM}s and gained similarity with T_{EX}s (Figure 4F). T_{CM}→Arm C4 cells corresponded equally to T_{CM} and T_{EM} (Figure 4F). Moreover, T_{CM}→Arm memory included fewer C4 cells (9.2%) compared with primary Arm memory cells (54.3%) (Table S1). These data were consistent with the progressive reduction in T_{CM} formation during serial transfers (Jabbari and Harty, 2006) and suggested that repeated stimulation resulted in the progressive differentiation of T_{CM}s.

LCMV cl13-derived cells (C2 and C5) were distinct from Arm-immune cells and distinguished by expression of the co-inhibitory receptor *Pdcd1* (PD-1) or the transcription factor *Tox* (Figures 4B, 4C, and S5C). The transcriptome of cl13-derived C5 cells corresponded to that of T_{ML} (Figure 4D), which is characterized by high *Tcf7*, *Id3*, and *Slamf6* (Ly108) expression (Figures S5B and S5D), whereas C2 cells corresponded to T_{EX} (Figure 4D), as exemplified by low *Tcf7* and high *GzmB* and *Cx3cr1* expression (Figure S5B). The T_{ML}→Arm memory compartment was distinct from both T_{ML} (C5) and T_{EX} cells (C2), but overlapped with Arm-immune cells (Figures 4C and 4E). The transcriptome of T_{ML}→Arm C1 cells corresponded weakly to T_{EM}, whereas T_{ML}→Arm C4 cells corresponded mainly to T_{CM} (Figure 4F). Thus, T_{ML}-derived memory cells were globally similar to T_{CM}-derived memory cells but were less differentiated.

Despite their overall similarity, T_{CM}→Arm C1 and T_{ML}→Arm differed in the expression of a significant number of genes (n = 64 among C1 cells and n = 79 among C4 cells (Table S2)). The hallmark Allograft Rejection was the most enriched gene signature in T_{CM}→Arm memory cells (both in C1 and C4) (Figures 4G and S5E). Indeed, these cells overexpressed effector genes including *Klrg1*, *GzmB and Id2* (Figure 4H; Table S2). On the other hand, T_{ML}→Arm memory cells overexpressed the central memory genes *Tcf7* (only C1), *Eomes*, *Id3* and *Sell* (only C4) (Figure 4I; Table S2).

The PID_ATF2 pathway was the most enriched gene signature in T_{ML}→Arm memory cells (both in C1 and C4) (Figures 4G and S5E). Furthermore, these cells overexpressed the exhaustion associated transcription factors *Nr4a2* (Chen et al., 2019) and *Tox* (Khan et al., 2019) (Figure 4J; Table S2). Thus, scRNA-seq analyses showed that T_{ML}-derived memory cells overlapped with conventional memory cells but showed a reduced bias toward effector differentiation and retained features of chronically stimulated cells.

The T_{CM}→Arm memory compartment harbored an additional cluster of cells (C6) (5.2%) (Figure 4E; Table S1). The transcriptome of these cells did not significantly overlap with any of the signatures tested in (Figure 4D) but showed an increase of the Hallmark signature Allograft Rejection compared to T_{CM}→Arm C1 cells. The identity and role of these cells remains to be addressed further.

Constitutive Tox expression mediates the chronic infection imprint seen in T_{ML}-derived memory cells

A prominent feature of T_{ML}→Arm memory cells was the constitutive expression of Tox. We thus addressed whether Tox expression explained the chronic infection imprint of these cells. To this end, we transduced *Tcf7*^{GFP} reporter P14 cells with an empty control (ctrl) or a Tox-expressing (Tox) mCherry retrovirus (Figure S6A) followed by their transfer into LCMV Arm-infected B6 mice. The abundance of Tox-expressing (mCherry^{+}) P14 memory cells at d28 p.i. was comparable to that of control transduced cells (Figure 5A), whereby Tox expression modestly increased the fraction of *Tcf7*$^{GFP+}$ (T_{CM}) relative to *Tcf7*$^{GFP-}$ (T_{EM}) memory cells (Figure 5B). Although CD127 and CD62L expression was not different (Figure S6B), fewer Tox^{+} *Tcf7*$^{GFP-}$ cells expressed KLRG1 (Figure 5C), indicating reduced differentiation. Furthermore, Tox^{+} memory cells (both *Tcf7*$^{GFP+}$ and *Tcf7*$^{GFP-}$) expressed more PD-1 (but not other markers of chronic infection) (Figures 5D and S6C) and produced less TNF-α and IL-2 (but comparable IFN-γ) compared with the corresponding control-transduced cells (Figure 5E). These data showed, in part, distinct effects of enforced Tox expression on T_{CM} and T_{EM}, confirming and extending reported effects in effector cells (Khan et al., 2019). Finally, we determined the recall response of Tox-expressing *Tcf7*$^{GFP+}$ memory cells. Although the expansion and formation of differentiated *Tcf7*$^{GFP-}$ progeny was similar, Tox^{+} (mCherry^{+}) *Tcf7*$^{GFP+}$ memory cells yielded more *Tcf7*$^{GFP+}$ progeny than control cells did (Figures 5F and 5G). The secondary cells expressing Tox showed reduced KLRG1 and increased PD-1 levels (Figure 5H). We concluded that constitutive Tox expression conferred, to a significant extent, the chronic infection imprint observed in T_{ML}-derived

Figure 3. T_{ML} cells yield a memory compartment with an imprint of prior chronic stimulation

(A and B) T_{CM} (Arm *Tcf7*$^{GFP+}$) and T_{ML} (cl13 *Tcf7*$^{GFP+}$) P14 cells (CD45.2^{+}) were flow sorted on d 42 p.i. and transferred into B6 recipients (CD45.1/2), which were then infected with LCMV Arm. Abundance (A) and expression of *Tcf7*^{GFP} (B) by T_{CM}→Arm and T_{ML}→Arm memory cells at d 50 p.i. The numbers in the bar graphs depict the mean fold difference between T_{CM}→Arm and T_{ML}→Arm P14 memory cells.

(C and D) *Tcf7*$^{GFP+}$ and *Tcf7*$^{GFP-}$ (or Tcf1^{+} and Tcf1^{-}) P14 cells were analyzed separately for the expression of the exhaustion/T_{ML} markers PD-1, LAG-3, Ly108, and CXCR5 (C) and Tox (D).

(E) Splenocytes were restimulated with gp33 peptide *in vitro* and P14 cells were analyzed for the production of IFN-γ, TNF-α, and IL-2.

(F and G) T_{CM}→Arm *Tcf7*$^{GFP+}$ and T_{ML}→Arm *Tcf7*$^{GFP+}$ memory cells (CD45.2^{+}) were flow sorted and transferred into tertiary B6 recipients (CD45.1), which were infected with LCMV Arm. Splenocytes were analyzed 8 days later for the abundance of tertiary P14 cells (F) and the presence of *Tcf7*$^{GFP+}$ cells (G). The numbers in the bar graphs depict the mean fold difference between tertiary cells of the indicated type.

Data in (A)–(D) and (E) are representative of three experiments with n = 4–7 mice per group. Data in (D) are representative of two experiments with n = 4–5 mice per group. Data in (F) and (G) are compiled from two experiments with n = 10 mice per group. All error bars are SD. Statistics are based on unpaired two-tailed Student's t test (A, B, F, and G) or on ANOVA with Fisher's exact test (C–E), whereby significance between the indicated groups is shown as *p < 0.05, **p < 0.01, ***p < 0.001; and ns (p > 0.05).

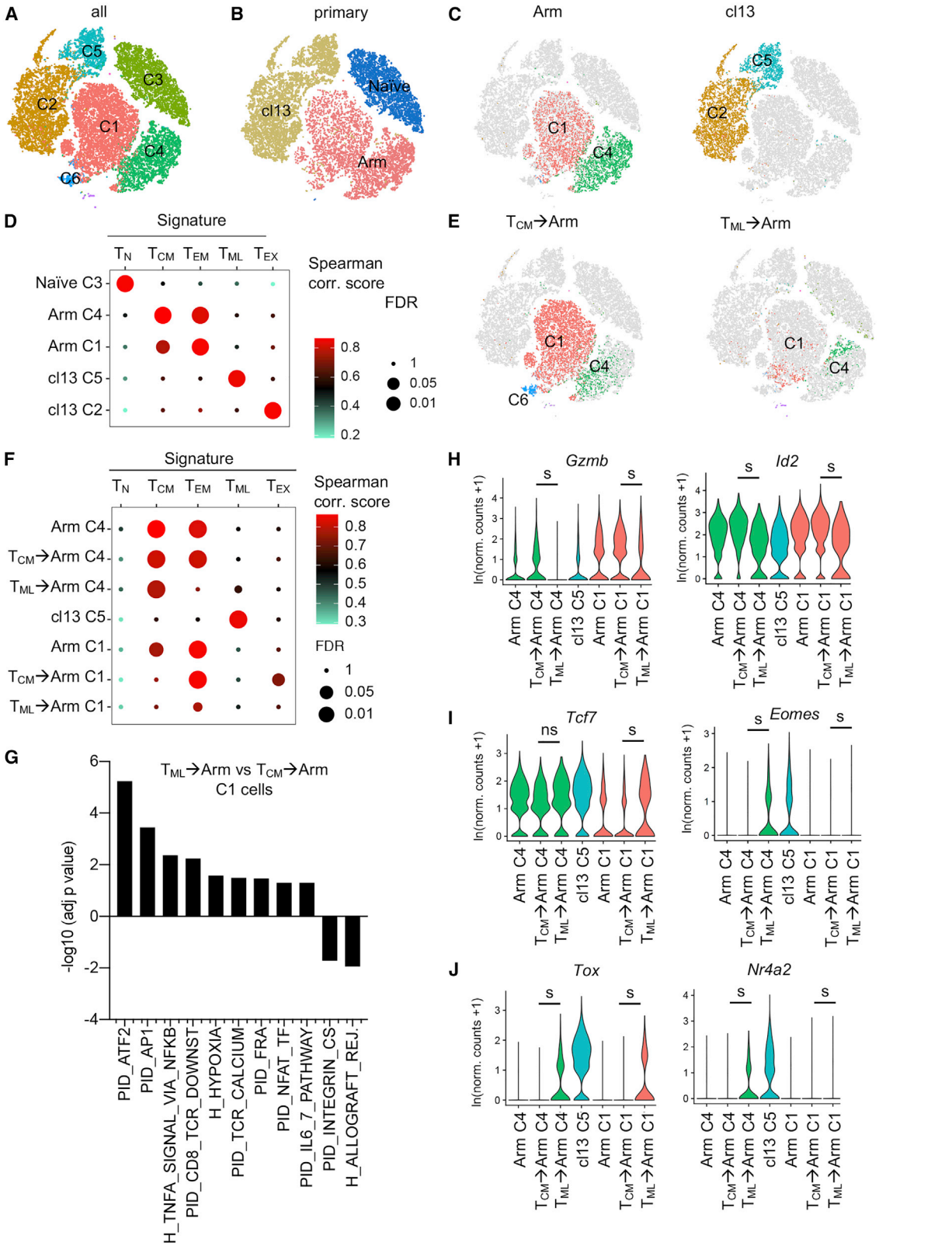

(legend on next page)

memory cells, including increased reproduction of *Tcf7*$^{GFP+}$ cells, reduced KLRG1, and increased PD-1 expression, as well as reduced cytokine production.

Virus-specific CD8$^+$ T cells that persist after clearance of systemic viral infection protect, in part, against re-infection

Finally, we investigated the virus-specific polyclonal CD8$^+$ T cells that persisted after the clearance of systemic LCMV cl13 infection and addressed whether such cells protected from renewed virus exposure. During chronic LCMV cl13 infection, polyclonal CD8$^+$ T cells specific for defined LCMV epitopes (gp33 and gp276) harbor *Tcf7*^{GFP}-defined T_{ML} and T_{EX} compartments very similar to monoclonal P14 cells (Utzschneider et al., 2016). Systemic LCMV cl13 infection is cleared around 6 weeks after infection, dependent on the neutralizing antibodies (Bergthaler et al., 2009), although infectious particles can be detected in the kidney for >100 days (Wherry et al., 2003). Following clearance of systemic LCMV cl13 infection (>d 88 p.i.) (Figure S7A), gp33- and gp276-specific CD8$^+$ T cells were readily detected. and their abundance was similar to that in Arm-immune mice (Figure S7B). in agreement with Wherry et al. (2003). Considerable fractions of the virus-specific CD8$^+$ T cells were *Tcf7*$^{GFP+}$ (Figure S7C). Despite clearance of systemic cl13 infection, PD-1, and Tox, but not LAG3, expression remained increased compared with Arm-immune cells (Figures S7D and S7E and not shown, respectively). To address the functional capacity of virus-specific *Tcf7*$^{GFP+}$ CD8$^+$ T cells, we flow sorted non-naive (CD44$^+$) *Tcf7*$^{GFP+}$ CD8$^+$ T cells (CD45.2) (containing known numbers of gp33- and gp276-specific cells) (Figure 6A) and transferred them into Vβ5 mice (CD45.1), which were infected with the LCMV Arm. Eight days later, gp33-specific *Tcf7*$^{GFP+}$ cells from Arm-immune mice had expanded 3.2-fold more than those from mice with cleared cl13 infection (Figure 6B). This was based on a reduced generation of differentiated *Tcf7*$^{GFP-}$ cells, whereas secondary *Tcf7*$^{GFP+}$ gp33$^+$ cells were comparably abundant (Figure 6C). Secondary gp33$^+$ cells did not differ in the expression of CD127, CD62L, and KLRG1 (not shown), but gp33$^+$ cells derived from cleared cl13 infection expressed more PD-1, LAG3, and Tox compared with those derived from the Arm-immune mice (Figure 6D). Corresponding data were obtained for gp276-specific CD8$^+$ T cells (Figures 6B and 6C and not shown). Similar to T_{ML}-derived *Tcf7*$^{GFP+}$ memory cells generated in response to recall stimulation, polyclonal *Tcf7*$^{GFP+}$ CD8$^+$ T cells that persisted after clearance of systemic infection retained evidence of prior chronic antigen exposure, suggesting that the latter cells also derived from T_{ML}.

Finally, we determined whether the *Tcf7*$^{GFP+}$ CD8$^+$ T cells that had previously responded to chronic infection protected against renewed infection. As expected, Vβ5 mice had high splenic virus titers at d 8 after LCMV-Arm infection and the transfer of Arm-immune, non-naive (CD44$^+$) *Tcf7*$^{GFP+}$ cells mediated efficient virus control. In comparison, CD44$^+$ *Tcf7*$^{GFP+}$ cells that had previously responded to LCMV cl13 infection mediated significant although more limited virus control (Figure 6E). These analyses suggested that *Tcf7*$^{GFP+}$ memory CD8$^+$ T cells that persist after clearance of systemic chronic infection have significant protective capacity against viral relapse or re-infection.

DISCUSSION

The fate of exhausted CD8$^+$ T cells after clearance of chronic infection is of clinical relevance because it provides information regarding possible protection from renewed virus exposure. The immune response to chronic viral infection is sustained by memory-like CD8$^+$ T cells (T_{ML}s), which combine characteristics of exhausted (e.g., PD-1) and memory CD8$^+$ T cells (e.g., Tcf1) (Utzschneider et al., 2016) (Im et al., 2016). However, the fate of these T_{ML}s after cessation of persistent antigen exposure has not been defined. Here, we show that T_{ML}s can form memory after antigen withdrawal and in response to acute, resolved infection. T_{ML}-derived memory cells resemble conventional central (T_{CM}) and effector memory cells (T_{EM}s) that arise in response to acute, resolved infection. Thus, chronic antigen exposure does not preclude the formation of a long-lived memory CD8$^+$ T cell compartment. However, in contrast to conventional memory cells, T_{ML}-derived memory cells maintained a stable phenotypic, transcriptional, and functional imprint of the original chronic antigen infection. Similar features were observed among virus-specific Tcf1$^+$ CD8$^+$ T cells that persisted after the

Figure 4. scRNA-seq analysis of the T_{ML}-derived memory cells

T_{CM} or T_{ML} P14 cells (CD45.2$^+$) were flow sorted on d 45 p.i. and transferred into B6 recipients (CD45.1/2), which were infected with LCMV Arm. Total splenic T_{CM}→Arm or T_{ML}→Arm P14 cells were flow sorted on d 42 p.i. and subjected to scRNA-seq analysis.

(A) t-distributed stochastic neighbor embedding (t-SNE) projection of all P14 cells, colored according to their cluster annotation.

(B) t-SNE projection of naive P14 cells (naive) and P14 cells responding to Arm or cl13 infection, colored according to their library annotation.

(C) t-SNE projection of P14 cells responding to Arm (left) or cl13 (right) infection, colored according to their cluster annotation.

(D) The transcriptomes of the cells from indicated clusters were tested for their correlation with gene signatures characteristic of naive (T_N), central memory (T_{CM}), effector memory (T_{EM}), memory-like (T_{ML}), or exhausted (T_{EX}) CD8$^+$ T cells (Utzschneider et al., 2016). The dot color depicts the Spearman correlation score, and the dot size indicates the false-discovery rate (FDR).

(E) t-SNE projection of T_{CM}→Arm (left) and T_{ML}→Arm memory cells (right), colored according to their cluster annotation.

(F) The transcriptomes of the cells from the indicated clusters were tested for their correlation with gene signatures characteristic of naive (T_N), central memory (T_{CM}), effector memory (T_{EM}), memory-like (T_{ML}), or exhausted (T_{EX}) CD8$^+$ T cells (Utzschneider et al., 2016). The dot color depicts the Spearman correlation score, and the dot size indicates the FDR.

(G) Genes differentially expressed between T_{ML}→Arm and T_{CM}→Arm cells that were both part of C1 were subjected to pathway analysis using the Pathway Interaction Database (PID_) and the Hallmark (H_) gene signatures. The graph shows the enrichment ($-\log_{10}$-adjusted p values) for the indicated signature.

(H–J) Violin plots show the expression level distribution of effector genes (H), memory genes (I), and exhaustion genes (J) in the indicated cell clusters based on scRNA-seq analysis, quantified by the normalized gene expression ($\log_2$ counts per million [cpm] +1).

Statistics are based on the Wilcoxon test, whereby significance between the indicated groups is shown as significant when $p < 0.05$ and ns when $p > 0.05$.

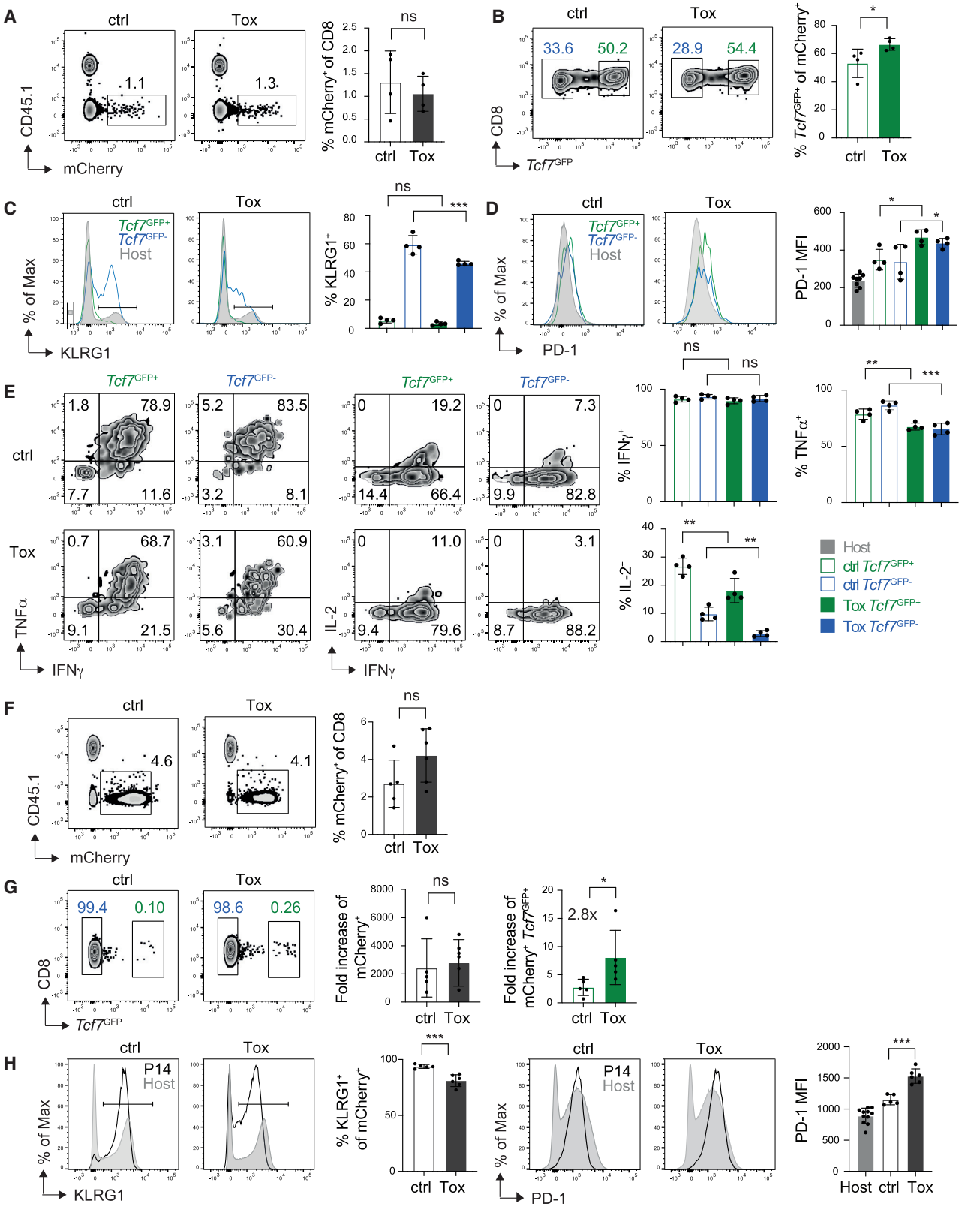

(legend on next page)

clearance of systemic viral infection, suggesting that these cells also derive from T_{ML}s.

Similar to chronic LCMV infection, the $CD8^+$ T cell response to chronic hepatitis C virus (HCV) infection contains epitope-specific PD-1^+ TCF1^+ (T_{ML}) and PD-1^+ TCF1^- (T_{EX}) compartments (Utzschneider et al., 2016) (Wieland et al., 2017). The emergence of virus-epitope-escape mutants suggests a critical role of the $CD8^+$ T cell response in HCV control. Like chronic LCMV, chronic HCV infection can resolve spontaneously, likely also dependent on the production of neutralizing antibodies (Kinchen et al., 2018). In addition, HCV can be cured using direct acting antiviral (DAA) agents. Interestingly, HCV epitope-specific $CD8^+$ T cells persist after resolved and cured HCV (Wieland et al., 2017). However, the origin and the functionality of the persisting $CD8^+$ T cells have remained unclear. Although it is possible that they derive from T_{ML}s, they may also derive from naive thymic $CD8^+$ T cell emigrants that were primed when the antigen load was already low and/or were exposed to antigen for limited periods of time. Indeed, virus-specific $CD8^+$ T cells that are primed after the establishment of chronic LCMV infection also preferentially generate T_{ML}-like cells, but these are less exhausted and more responsive to immunotherapy (Snell et al., 2018). To formally exclude a potential contribution of recent thymic emigrants and to ensure that persisting $CD8^+$ T cells derive from T_{ML}s, we have initially used adoptive T_{ML} transfers into antigen-free hosts and T_{ML} restimulation by acute, resolved infection in secondary hosts. We found that T_{ML} persisted upon antigen withdrawal and that they maintained the expression of multiple markers expressed by chronically stimulated cells and T_{ML}, including PD-1, CXCR5. and Ly108. This suggested that the T_{ML} phenotype represented a stable state that did not depend on continuous antigen exposure. After acute restimulation, T_{ML}-derived memory cells adopted features of conventional memory cells, which, nevertheless, expressed markers of chronically stimulated cells, including Tox, demonstrating that aspects of a chronic infection phenotype was maintained through cell division. These data formally showed that T_{ML} had the potential to yield long-lived memory compartment but that such cells maintained a stable imprint of the initial chronic antigen exposure. When this manuscript was under revision, it was reported that HCV epitope-specific $CD8^+$ T cells that persist after DAA-mediated HCV elimination expressed Tcf1 and had a chronic infection phenotype. In addition, in part, identical clonotypes were detectable during chronic infection (Hensel et al., 2021). These findings suggested that the persisting cells derived from T_{ML}s. Collectively, the data show that characteristics of chronically stimulated $CD8^+$ T cells are stably maintained after antigen withdrawal, natural resolution of chronic infection, drug-mediated virus elimination, and even recall stimulation.

Our scRNA-seq analyses showed that *Tox* expression differentiated T_{ML}- from T_{CM}-derived memory cells. Persistent TOX expression was similarly observed in drug-cured HCV (Hensel et al., 2021). To address the relevance of this finding we transduced virus-specific $CD8^+$ T cells with a Tox expression construct before their stimulation by acute, resolved infection. Tox expression in conventional memory cells (T_{CM}s and T_{EM}s) increased inhibitory receptor expression (PD-1 and LAG3) and reduced cytokine production (TNF-α and IL-2 production), consistent with prior analyses of Tox-transduced effector cells (Khan et al., 2019). Thus, elevated Tox expression recapitulated most of the chronic-infection-associated changes observed in T_{ML}-derived memory cells.

Despite overall similarities, persisting virus-specific $CD8^+$ T cells seemed to differ depending on how the antigen was removed. For example, T_{ML}-derived memory cells globally resembled conventional memory cells. That was similar for HCV-specific $CD8^+$ T cells persisting after resolution of HCV infection (Hensel et al., 2021). In contrast, HCV-specific $CD8^+$ T cells that persisted after drug-mediated virus elimination corresponded to chronically stimulated cells. Immune-mediated (T cell or B cell), rather than drug-dependent, antigen removal may, thus, be needed for the conversion of T_{ML}s into more conventional memory cells. Further, T_{CM}- and T_{ML}-derived Tcf1^+ memory cells had a comparable capacity to generate effector cells in response to re-infection. In comparison, Tcf1^+ cells from mice with cleared systemic LCMV infection had a reduced ability to generate effector cells. The latter may be due to antigen persistence in those mice, leading to the occasional stimulation of virus-specific $CD8^+$ T cells. Alternatively, it was possible that recall stimulation was required to fully correct the expansion/differentiation defect of T_{ML}s. Numerous factors may fine-tune the fate, the imprint, and the functionality of the persisting virus-specific $CD8^+$ T cells. Such factors likely include the time, extent, and context of the primary antigen exposure; the time after antigen removal; whether the antigen has been completely cleared; whether the antigen clearance was drug or immune mediated; and whether cells underwent recall expansion.

Independent of the above differences, it is important to address whether the chronic-infection imprint affected the

Figure 5. Enforced Tox expression reproduces features of T_{ML}-derived memory cells

(A and B) *Tcf7*^{GFP} P14 cells (CD45.2) were transduced *in vitro* with a control (ctrl) or a Tox-expressing (Tox) mCherry retrovirus and transferred into Arm-infected B6 mice (CD45.1/2); 28 days later, $CD8^+$ T cells were analyzed for the presence of mCherry$^+$ P14 cells (A) and the presence of *Tcf7*$^{GFP+}$ (T_{CM}) cells (B) among gated mCherry$^+$ P14 cells.

(C and D) MCherry$^+$ *Tcf7*$^{GFP+}$ (T_{CM}) and mCherry$^+$ *Tcf7*$^{GFP-}$ (T_{EM}) cells were then analyzed separately for KLRG1 (C) and PD-1 (D) expression.

(E) Splenocytes were restimulated with gp33 peptide *in vitro*, and mCherry$^+$ P14 cells were analyzed for the production of IFN-γ, TNF-α, and IL-2.

(F and G) Recall response of flow sorted *Tcf7*$^{GFP+}$ mCherry$^+$ P14 cells at d 8 after transfer into new B6 hosts and Arm infection (d 28 + 8). Abundance of mCherry$^+$ P14 cells among gated $CD8^+$ T cells (F) and *Tcf7*$^{GFP+}$cells among mCherry$^+$ P14 cells (G). The fold increase of the cells was calculated relative to the input, assuming a 10% take of the transferred cells.

(H) Secondary mCherry$^+$ cells were analyzed for KLRG1 and PD-1 expression.

Data are representative of three independent experiments, each with n = 2–5 mice per group. All error bars are SD. Statistics are based on unpaired two-tailed Student's t test (A, B, and F–H) or on ANOVA with Fisher's exact test (C–E), whereby significance among the indicated groups is shown as *$p < 0.05$, **$p < 0.01$, ***$p < 0.001$; and ns ($p > 0.05$).

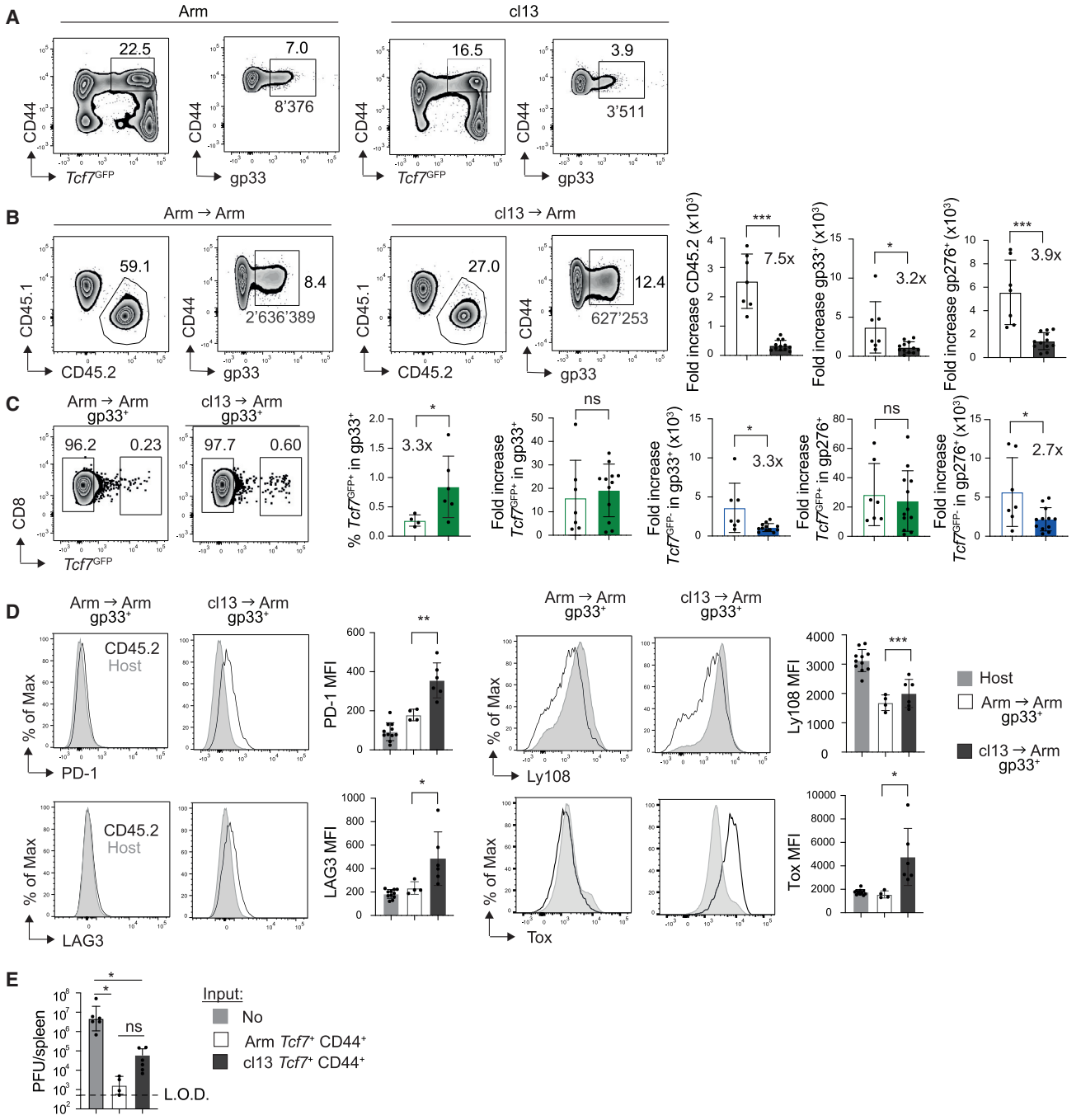

Figure 6. Virus-specific CD8⁺ T cells that persist after clearance of systemic viral infection retain features of chronically stimulated CD8⁺ T cells

B6 *Tcf7*^{GFP} mice were infected with LCMV Arm or LCMV cl13 and analyzed at >d 88 p.i. when systemic LCMV cl13 infection had been cleared.

(A) CD44⁺ *Tcf7*$^{GFP+}$ CD8⁺ T cells (CD45.2) were flow sorted, and 10^5 cells containing a known number of gp33 (and gp276)-specific CD8⁺ T cells were transferred into Vβ5 mice (CD45.1), which were then infected with LCMV Arm.

(B and C) Eight days later (>d 88 + 8), CD45.2⁺ cells were analyzed for the presence of gp33⁺ (and gp276⁺) cells (B) and the expression of *Tcf7*^{GFP} by antigen-specific cells (C). The fold expansion of CD45.2⁺, gp33⁺ and gp33⁺ *Tcf7*⁺, and gp276⁺ and gp276⁺ *Tcf7*⁺ cells were calculated relative to input (assuming a take of 10%). The numbers in the bar graphs depict the mean fold difference between the indicated type of Arm→Arm and cl13→Arm cells.

(D) gp33⁺ cells were analyzed for the expression of PD-1, LAG3, Ly108, and Tox.

(E) The spleens of recipient Vβ5 mice that had received no cell transfer (No), Arm-immune CD44⁺ *Tcf7*$^{GFP+}$ CD8⁺ T cells, or the corresponding cells from resolved cl13 infection and that had been infected with LCMV Arm were analyzed for infectious LCMV at d 8 p.i., depicted as plaque-forming units (PFU) per spleen. The broken line depicts the limit of detection (LOD).

(legend continued on next page)

protective capacity of persisting CD8$^+$ T cells. Indeed, anecdotal evidence suggests that viral relapse after DAA-mediated HCV cure induces a recall response that is, however, unable to control the infection (Wieland et al., 2017). We found that renewed virus challenge resulted in a recall response and in significant virus control, although more limited compared with conventional memory CD8$^+$ T cells. These data showed that resolution of systemic infection yields a long-lived CD8$^+$ T cell compartment that has protective capacity.

Collectively, we show that T_{ML}s can yield long-lived memory cells that resemble conventional memory cells but that keep a transcriptional and phenotypic imprint of prior chronic stimulation. Nevertheless, these cells can mediate a recall response and can significantly reduce renewed viral infection. Thus, the immune system remembers prior acute, as well as prior chronic, infection, whereby the prior infection affects the quality of the secondary response and the protection from renewed infection.

STAR★METHODS

Detailed methods are provided in the online version of this paper and include the following:

- KEY RESOURCES TABLE
- RESOURCE AVAILABILITY
  - Lead contact
  - Materials availability
  - Data and code availability
- EXPERIMENTAL MODEL AND SUBJECT DEAILS
- METHOD DETAILS
  - Viral infections
  - Adoptive T cell transfer
  - Cell suspension, surface and intracellular staining, flow cytometry and cell sorting
  - Retroviral viral vectors, virus production and T cell transduction
  - Single cell RNA sequencing analysis
- QUANTIFICATION AND STATISTICAL ANALYSIS

SUPPLEMENTAL INFORMATION

Supplemental information can be found online at https://doi.org/10.1016/j.celrep.2021.109672.

ACKNOWLEDGMENTS

We thank D. Pinschewer, Universität Basel, for providing LCMV cl13 Δgp33; R. Veber for critically reading the manuscript; C. Fumey for mouse management; B. Mangeat and the Gene Expression Core Facility (GECF), EPFL School of Life Sciences for-single cell RNA sequencing; and the University of Lausanne Flow Cytometry Facility for expert assistance with flow cytometry. W.H. is supported in part by a grant from the Swiss National Science Foundation (SNSF) (310030B_179570).

AUTHOR CONTRIBUTIONS

M.C. performed and analyzed all wet laboratory experiments and prepared figures; T.W. performed bioinformatics analysis and prepared figures; M.D. supervised bioinformatics analysis; and W.H. conceived and supervised the study and wrote the paper.

DECLARATION OF INTERESTS

The authors declare no competing interests.

Received: June 4, 2020
Revised: June 28, 2021
Accepted: August 16, 2021
Published: September 7, 2021

REFERENCES

Alfei, F., Kanev, K., Hofmann, M., Wu, M., Ghoneim, H.E., Roelli, P., Utzschneider, D.T., von Hoesslin, M., Cullen, J.G., Fan, Y., et al. (2019). TOX reinforces the phenotype and longevity of exhausted T cells in chronic viral infection. Nature *571*, 265–269.

Angelosanto, J.M., Blackburn, S.D., Crawford, A., and Wherry, E.J. (2012). Progressive loss of memory T cell potential and commitment to exhaustion during chronic viral infection. J. Virol. *86*, 8161–8170.

Aran, D., Looney, A.P., Liu, L., Wu, E., Fong, V., Hsu, A., Chak, S., Naikawadi, R.P., Wolters, P.J., Abate, A.R., et al. (2019). Reference-based analysis of lung single-cell sequencing reveals a transitional profibrotic macrophage. Nat. Immunol. *20*, 163–172.

Battagay, M., Cooper, S., Althage, A., Banziger, J., Hengartner, H., and Zinkernagel, R., M. (1991). Quantification of lymphocytic choriomeningitis virus with an immunological focus assay in 24- or 96-well plates. J. Virol. Meth. *33*, 191–198.

Benjamini, Y., and Hochberg, Y. (1995). Controlling the false discovery rate: a practical and powerful approach to multiple testing. J. R. Stat. Soc. Series B Stat. Methodol. *57*, 289–300.

Bergthaler, A., Flatz, L., Verschoor, A., Hegazy, A.N., Holdener, M., Fink, K., Eschli, B., Merkler, D., Sommerstein, R., Horvath, E., et al. (2009). Impaired antibody response causes persistence of prototypic T cell-contained virus. PLoS Biol. *7*, e1000080.

Blank, C.U., Haining, W.N., Held, W., Hogan, P.G., Kallies, A., Lugli, E., Lynn, R.C., Philip, M., Rao, A., Restifo, N.P., et al. (2019). Defining "T cell exhaustion.". Nat. Rev. Immunol. *19*, 665–674.

Chen, J., López-Moyado, I.F., Seo, H., Lio, C.J., Hempleman, L.J., Sekiya, T., Yoshimura, A., Scott-Browne, J.P., and Rao, A. (2019). NR4A transcription factors limit CAR T cell function in solid tumours. Nature *567*, 530–534.

Dillon, S.R., Jameson, S.C., and Fink, P.J. (1994). V beta 5+ T cell receptors skew toward OVA+H-2Kb recognition. J. Immunol. *152*, 1790–1801.

Doering, T.A., Crawford, A., Angelosanto, J.M., Paley, M.A., Ziegler, C.G., and Wherry, E.J. (2012). Network analysis reveals centrally connected genes and pathways involved in CD8$^+$ T cell exhaustion versus memory. Immunity *37*, 1130–1144.

Hensel, N., Gu, Z., Sagar, Wieland, D., Jechow, K., Kemming, J., Llewellyn-Lacey, S., Gostick, E., Sogukpinar, O., Emmerich, F., et al. (2021). Memory-like HCV-specific CD8$^+$ T cells retain a molecular scar after cure of chronic HCV infection. Nat. Immunol. *22*, 229–239.

Data in (A)–(C) are compiled from two independent experiments with n = 7 LCMV Arm and n = 12 LCMV cl13 infected mice. Data in (D) and (E) are from one representative experiment of two performed with each having three or more mice per group. All error bars are SD. Statistics are based on unpaired two-tailed Student's t test (B–D) or on ANOCA with Fisher's exact test (E), whereby significance between the indicated groups is shown as *$p < 0.05$, **$p < 0.01$, ***$p < 0.001$; and ns ($p > 0.05$).

Hudson, W.H., Gensheimer, J., Hashimoto, M., Wieland, A., Valanparambil, R.M., Li, P., Lin, J.X., Konieczny, B.T., Im, S.J., Freeman, G.J., et al. (2019). Proliferating transitory T Cells with an effector-like transcriptional signature emerge from PD-1^{+} stem-like CD8^{+} T cells during chronic infection. Immunity *51*, 1043–1058.e4.

Im, S.J., Hashimoto, M., Gerner, M.Y., Lee, J., Kissick, H.T., Burger, M.C., Shan, Q., Hale, J.S., Lee, J., Nasti, T.H., et al. (2016). Defining CD8^{+} T cells that provide the proliferative burst after PD-1 therapy. Nature *537*, 417–421.

Jabbari, A., and Harty, J.T. (2006). Secondary memory CD8^{+} T cells are more protective but slower to acquire a central-memory phenotype. J. Exp. Med. *203*, 919–932.

Johnson, S., Bergthaler, A., Graw, F., Flatz, L., Bonilla, W.V., Siegrist, C.-A., Lambert, P.-H., Regoes, R.R., and Pinschewer, D.D. (2015). Protective efficacy of individual CD8+ T cell specificities in chronic viral infection. J. Immunol. *194*, 1755–1762.

Kaech, S.M., and Cui, W. (2012). Transcriptional control of effector and memory CD8^{+} T cell differentiation. Nat. Rev. Immunol. *12*, 749–761.

Khan, O., Giles, J.R., McDonald, S., Manne, S., Ngiow, S.F., Patel, K.P., Werner, M.T., Huang, A.C., Alexander, K.A., Wu, J.E., et al. (2019). TOX transcriptionally and epigenetically programs CD8^{+} T cell exhaustion. Nature *571*, 211–218.

Kinchen, V.J., Zahid, M.N., Flyak, A.I., Soliman, M.G., Learn, G.H., Wang, S., Davidson, E., Doranz, B.J., Ray, S.C., Cox, A.L., et al. (2018). Broadly neutralizing antibody mediated clearance of human hepatitis C virus infection. Cell Host Microbe *24*, 717–730.e5.

Liberzon, A., Birger, C., Thorvaldsdóttir, H., Ghandi, M., Mesirov, J.P., and Tamayo, P. (2015). The Molecular Signatures Database (MSigDB) hallmark gene set collection. Cell Syst. *1*, 417–425.

Pais Ferreira, D., Gomes Silva, J., Wyss, T., Fuertes Marraco, S.A., Scarpellino, L., Charmoy, M., Maas, R., Siddiqui, I., Tang, L., Joyce, J.A., et al. (2020). Central memory CD8 $^{+}$ T cells derive from stem-like Tcf7 ^{hi} effector cells in the absence of cytotoxic differentiation. Immunity *53*, 985–1000.e11.

Robinson, M.D., McCarthy, D.J., and Smyth, G.K. (2010). edgeR: a Bioconductor package for differential expression analysis of digital gene expression data. Bioinformatics *26*, 139–140.

Sallusto, F., Lenig, D., Förster, R., Lipp, M., and Lanzavecchia, A. (1999). Two subsets of memory T lymphocytes with distinct homing potentials and effector functions. Nature *401*, 708–712.

Scott, A.C., Dündar, F., Zumbo, P., Chandran, S.S., Klebanoff, C.A., Shakiba, M., Trivedi, P., Menocal, L., Appleby, H., Camara, S., et al. (2019). TOX is a critical regulator of tumour-specific T cell differentiation. Nature *571*, 270–274.

Shin, H., Blackburn, S.D., Blattman, J.N., and Wherry, E.J. (2007). Viral antigen and extensive division maintain virus-specific CD8 T cells during chronic infection. J. Exp. Med. *204*, 941–949.

Snell, L.M., MacLeod, B.L., Law, J.C., Osokine, I., Elsaesser, H.J., Hezaveh, K., Dickson, R.J., Gavin, M.A., Guidos, C.J., McGaha, T.L., and Brooks, D.G. (2018). CD8^{+} T cell priming in established chronic viral infection preferentially directs differentiation of memory-like cells for sustained immunity. Immunity *49*, 678–694.e5.

Stuart, T., Butler, A., Hoffman, P., Hafemeister, C., Papalexi, E., Mauck, W.M., III, Hao, Y., Stoeckius, M., Smibert, P., and Satija, R. (2019). Comprehensive integration of single-cell data. Cell *177*, 1888–1902.e21.

Subramanian, A., Tamayo, P., Mootha, V.K., Mukherjee, S., Ebert, B.L., Gillette, M.A., Paulovich, A., Pomeroy, S.L., Golub, T.R., Lander, E.S., and Mesirov, J.P. (2005). Gene set enrichment analysis: a knowledge-based approach for interpreting genome-wide expression profiles. Proc. Natl. Acad. Sci. USA *102*, 15545–15550.

Utzschneider, D.T., Legat, A., Fuertes Marraco, S.A., Carrié, L., Luescher, I., Speiser, D.E., and Zehn, D. (2013). T cells maintain an exhausted phenotype after antigen withdrawal and population reexpansion. Nat. Immunol. *14*, 603–610.

Utzschneider, D.T., Charmoy, M., Chennupati, V., Pousse, L., Ferreira, D.P., Calderon-Copete, S., Danilo, M., Alfei, F., Hofmann, M., Wieland, D., et al. (2016). T cell factor 1-expressing memory-like CD8^{+} T cells sustain the immune response to chronic viral infections. Immunity *45*, 415–427.

van der Maaten, L.J.P., and Hinton, G.E. (2008). Visualizing data using t-SNE. J. Mach. Learn. Res. *9*, 2579–2605.

Wherry, E.J., and Kurachi, M. (2015). Molecular and cellular insights into T cell exhaustion. Nat. Rev. Immunol. *15*, 486–499.

Wherry, E.J., Blattman, J.N., Murali-Krishna, K., van der Most, R., and Ahmed, R. (2003). Viral persistence alters CD8 T-cell immunodominance and tissue distribution and results in distinct stages of functional impairment. J. Virol. *77*, 4911–4927.

Wieland, D., Kemming, J., Schuch, A., Emmerich, F., Knolle, P., Neumann-Haefelin, C., Held, W., Zehn, D., Hofmann, M., and Thimme, R. (2017). TCF1^{+} hepatitis C virus-specific CD8^{+} T cells are maintained after cessation of chronic antigen stimulation. Nat. Commun. *8*, 15050.

Wu, T., Ji, Y., Moseman, E.A., Xu, H.C., Manglani, M., Kirby, M., Anderson, S.M., Handon, R., Kenyon, E., Elkahloun, A., et al. (2016). The TCF1-Bcl6 axis counteracts type I interferon to repress exhaustion and maintain T cell stemness. Sci. Immunol. *1*, eeai8593.

Yao, C., Sun, H.W., Lacey, N.E., Ji, Y., Moseman, E.A., Shih, H.Y., Heuston, E.F., Kirby, M., Anderson, S., Cheng, J., et al. (2019). Single-cell RNA-seq reveals TOX as a key regulator of CD8^{+} T cell persistence in chronic infection. Nat. Immunol. *20*, 890–901.

Yu, G., Wang, L., G, Han, Y., and He, Q., Y. (2012). clusterProfiler: an R package for comparing biological themes among gene clusters. OMICS *16*, 284–287.

Zander, R., Schauder, D., Xin, G., Nguyen, C., Wu, X., Zajac, A., and Cui, W. (2019). CD4^{+} T cell help is required for the formation of a cytolytic CD8^{+} T cell subset that protects against chronic infection and cancer. Immunity *51*, 1028–1042.e4.

CellPress
OPEN ACCESS

STAR★METHODS

KEY RESOURCES TABLE

REAGENT or RESOURCE	SOURCE	IDENTIFIER
Antibodies		
Anti-Mouse CD8α – PerCP-Cy5.5 or APC-eF780	eBioscience	Clone 53.6.7; RRID: AB_1107004 RRID: AB_1272185
Anti-Mouse CD45.1 – Pacific Blue		Clone A20 In house
Anti-Mouse CD45.2– PerCP Cy5.5 or AlexaFluor 680	eBioscience	Clone 104.2; RRID: AB_953590 in house
Anti-Mouse CD62L – PE, Brilliant Violet 711	eBioscience / BioLegend	Clone Mel14; RRID: AB_465722 RRID: AB_2564215
Anti-Mouse CD127 APC or Brilliant Violet 785	eBioscience / BioLegend	Clone A7R34; RRID: AB_469435 RRID: AB_2565269
Anti-Mouse IFN-γ - PE	eBioscience	Clone XMG1.2; RRID: AB_466193
Anti-Mouse IL-2 – APC	eBioscience	Clone JES6-5H4; RRID: AB_2535421
Anti-Mouse TNFα – PE Cy7	eBioscience	Clone MP6-XT22; RRID: AB_11042471
Anti-Mouse CXCR5 PE	eBioscience	Clone: SPRCL5; RRID: AB_11217882
Anti-Mouse KLRG1 - PE Cy7, APC	eBioscience	Clone 2F1; RRID: AB_1518768 RRID: AB_469469
Anti-Mouse LAG3 PerCP-eFluor 710	eBioscience	Clone eBioC9B7W; RRID: AB_11151148
Anti-Mouse Ly108 biotin	eBioscience	Clone eBio13G3-19D; RRID: AB_763614
Anti-Mouse PD-1 PE/Cy7	BioLegend	Clone RMP1-30; RRID: AB_572017
Anti-Mouse/human TCF1 (rabbit mAb)	Cell Signaling Technology	Clone C63D9; RRID: AB_2199302
Anti-Mouse Tox – PE, eFluor660	eBioscience	Clone TXRX10; RRID: AB_10855034 RRID: AB_2574265
Granzyme B PE-Texas Red	Invitrogen	Clone GB11; RRID: AB_2536540
Anti-Mouse Ki67 – FITC	BD Biosciences	RRID: AB_396302
F(ab')2-Donkey anti-Rabbit IgG (H+L) – PE	eBioscience	RRID: AB_1210761
Goat anti-Rabbit IgG (H+L) -AF647	Molecular Probes (Invitrogen)	RRID: AB_141663
H-2D^b / gp33-41 – APC (Tetramer)	TC Metrix	N/A
H-2D^b /gp276 – APC (Tetramer)	TC Metrix	N/A
Streptavidin, Alexa Fluor 610	ThermoFisher Scientific	Cat# S20982
Bacterial and virus strains		
LCMV 53b Armstrong (Arm)	D. Zehn, IVR-CHUV	in house
LCMV Clone 13	D. Zehn, IVR-CHUV	in house
LCMV Clone 13 Δgp33	(Johnson et al., 2015)	In house
Chemicals, peptides, and recombinant proteins		
Ammonium-Chloride-Potassium (ACK) buffer	In house	N/A
Brefeldin A	Biolegend	Cat# 420601
Peptide: LCMV glycoprotein amino acids 33-41 (gp33) (KAVYNFATM)	TC Metrix	N/A
TurboFect Transfection Reagent	ThermoFisher Scientific	Cat# R0533
Polybrene	Sigma-Aldrich	Cat# TR-1003-G
Recombinant human IL-2	Glaxo IMB, Genève, Switzerland	gift from N. Rufer, UNIL/CHUV
7-AAD (Viability dye)	Biolegend	Cat# 420404
DAPI	Life Technologies	Cat# D1306
Critical commercial assays		
Mouse CD8$^+$ T cell enrichment kit	StemCell Technologies	Cat# 19853
Intracellular Fix & Perm Buffer set	eBiosciences	Cat# 88-8824

(*Continued on next page*)

Continued

REAGENT or RESOURCE	SOURCE	IDENTIFIER
FoxP3/Transcription factor staining buffer set	eBiosciences	Cat# 00-5523
Zombie Aqua Fixable Viability kit	Biolegend	Cat# 423101
Annexin V - APC Apoptosis Detection Kit	eBioscience	RRID: AB_2575165
Deposited data		
scRNASeq data	This study	GEO: GSE153376
Experimental models: Organisms and strains		
Mouse: C57BL/6 (B6) (CD45.2)	Charles River Laboratories	Strain 027
Mouse: B6.SJL-Ptprc < a > (B6 CD45.1)	Jackson Lab	Strain 002014; RRID: MGI:6200621
Mouse: B6.Tg(Tcf7^{GFP})Whe (*Tcf7*^{GFP}) (CD45.2)	(Utzschneider et al., 2016)	N/A
Mouse: Vb5 TCRb only transgenic (B6 CD45.1)	(Dillon et al., 1994).	N/A
Mouse: B6; D2-Tg(TcrLCMV)327Sdz P14 T cell receptor (TCR) transgenic (CD45.2)	H.P. Pircher, (Freiburg, Germany)	RRID: MGI_3810256
Recombinant DNA		
pMSCV-mCherry v2	Vectorbuilder	This study
pMSCV-mTox[NM_145711.5]:IRES:mCherry	Vectorbuilder	This study
pCL-Eco	I. Verma	RRID: Addgene_12371
Software		
GraphPad Prism v8	https://graphpad-prism.software.informer.com/5.0/	RRID: SCR_002798
FlowJo v10	Tree Star	RRID: SCR_008520
Adobe Illustrator v24.0.1	Adobe cloud	N/A
10x Cell Ranger v3.0.1		https://support.10xgenomics.com/single-cell-gene-expression/software/overview/welcome
R v4.0.3		https://cran.r-project.org/
Seurat v3.2.2	(Stuart et al., 2019)	https://cran.r-project.org/web/packages/Seurat/index.html
SingleR v1.4.0	(Aran et al., 2019)	https://bioconductor.org/packages/release/bioc/html/SingleR.html
clusterProfiler v3.18.0	(Yu et al., 2012)	https://bioconductor.org/packages/release/bioc/html/clusterProfiler.html

RESOURCE AVAILABILITY

Lead contact

Further information and requests may be directed to and will be fulfilled by the lead contact Werner Held (Werner.Held@unil.ch).

Materials availability

All stable reagents generated in this study are available from the lead contact with a completed Materials Transfer Agreement.

Data and code availability

Sequencing data generated in this study have been deposited into the GEO database with accession number GEO: GSE153376. This paper does not report original code. Any additional information required to reanalyze the data reported in this paper is available from the lead contact upon request.

EXPERIMENTAL MODEL AND SUBJECT DEAILS

Mouse strains were maintained in the SPF animal facility of the University of Lausanne. Both male and female mice between 6 and 12 weeks of age were used for experiments whereby donors and recipients were sex matched for adoptive T cell transfers. Animal experiments were conducted in accordance with protocols approved by the veterinary authorities of the Canton de Vaud.

C57BL/6 (B6) (CD45.2) were obtained from Charles River (L'Arbresle Cedex, France), CD45.1 congenic B6 mice were bred locally. P14 T cell receptor (TCR) transgenic mice (TCR specific for the LCMV gp33–41 epitope (gp33)), provided by H.P. Pircher (Freiburg, Germany), Vβ5 TCR transgenic mice (Dillon et al., 1994) provided by P. Fink (Seattle, USA). *Tcf7*^{GFP} reporter mice have been described (Utzschneider et al., 2016). P14 *Tcf7*^{GFP} mice were obtained by breeding.

METHOD DETAILS

Viral infections

Mice were infected intraperitoneally (i.p.) with 2 × 10^5 plaque forming units (pfu) of LCMV 53b Armstrong (Arm) strain, intravenously (i.v.) with 2x10^6 pfu of LCMV clone 13 (cl13) strain or i.v. with 200 pfu of LCMV cl13 Δgp33: (KAVYN(**F** → **L)**ATC) strain (Johnson et al., 2015). To determine viral titers, spleens from LCMV-infected mice were 'shock frozen'. Diluted spleen suspensions were then used to infect Vero cells, and viral titers were determined by an LCMV focus-forming assay, as described elsewhere (Battagay et al., 1991).

Adoptive T cell transfer

Tcf7^{GFP} P14 cells were obtained by mashing the spleen through a 40 μm nylon cell strainer (BD Falcon). Red blood cells were lysed with a hypotonic Ammonium-Chloride-Potassium (ACK) buffer. CD8$^+$ T cells were purified using mouse CD8$^+$ T cell enrichment kit (StemCell Technologies). Purified P14 cells (CD45.2) (10^4) (usually > 95% pure) were adoptively transferred intravenously (i.v.) into naive B6 (CD45.1 or CD45.1/2) or Vβ5 TCR transgenic B6 mice (CD45.1) one day prior to infection (d-1).

For secondary transfers of P14 cells, 2x10^3 to 10^4 flow sorted *Tcf7*$^{GFP+}$ P14 cells were transferred i.v. into naive B6 (CD45.1 or CD45.1/2) recipients. For transfers of polyclonal CD8$^+$ T cells, 10^5 flow sorted *Tcf7*$^{GFP+}$ CD44$^+$ CD8$^+$ T cells were transferred i.v. into naive Vβ5 (CD45.1) mice. For all experiments involving flow sorted cells, cell transfer and LCMV infections were done on the same day (d0).

Cell suspension, surface and intracellular staining, flow cytometry and cell sorting

Cell suspensions from the spleen were obtained by mashing through a 40μM nylon cell strainer, followed by red blood cells lysis using ACK buffer.

Surface staining was performed with mAbs for 20 min at 4°C in PBS supplemented with 2% FCS (FACS buffer) using the reagents in the Key resources table and Zombie Aqua Fixable Viability kit (Biolegend) was used to exclude dead cells. For tetramer staining, cell suspensions were incubated with anti-CD16/32 (2.4G2) hybridoma supernatant before staining for 90min at 4°C with APC-conjugated MHC-I tetramers.

For intranuclear staining, cells were surface stained before fixation and permeabilization using the Foxp3 transcription factor staining kit (eBioscience: Cat. No. 00-5523) followed by intranuclear staining in Permeabilization buffer 1x (Perm buffer).

For the detection of cytokine production, splenocytes were re-stimulated *in vitro* with LCMV gp33-41 (gp33) (1μM) peptide for 5h in the presence of Brefeldin A (5μg/ml) for the last 4.5h. Cells were then stained at the surface before fixation and permeabilization (using eBioscience kit: Cat. No. 88-8824) followed by intracellular staining in 1x Perm buffer.

Cell surface stained cells were analyzed directly. Flow cytometry measurements of cells were performed on an LSR-II or Fortessa flow cytometer (BD). Data were analyzed using FlowJo version10 (TreeStar).

For cell sorting of P14 cells, splenocytes were enriched for CD8$^+$ T cells using the mouse CD8$^+$ T cell enrichment kit (StemCell Technologies) and stained for CD45.1 (A20) or CD45.2 (clone 104). *Tcf7*$^{GFP+}$ CD45.1$^-$ CD45.2$^+$ P14 cells were flow sorted on a FACSAria (BD) flow cytometer.

For the analysis of engraftment, mice were injected i.v. with 3mg of APC-eF780-labeled anti-CD8α mAb (clone 53-6.7) 4 min prior to sacrifice. CD8α$^-$ cells were considered to be located in the white pulp of the spleen, while CD8α$^+$ cells were considered located in the red pulp.

Retroviral viral vectors, virus production and T cell transduction

pMSCV-IRES:mCherry and pMSCV-mTox:IRES:mCherry was synthesized by Vectorbuilder. For retrovirus (RV) production, 293T cells (passage number < 10) were transiently transfected with retrovirus vector plus a packaging plasmid (pCL-Eco) using Turbofect (ThermoFisher) in the absence of antibiotics. Culture supernatants were collected 48 h after transfection, filtered through a 0.45mM filter (Millex) and either used directly to transduce activated CD8$^+$T cells or stored frozen.

CD8$^+$T cells were purified from the spleen of naive P14 *Tcf7*^{GFP} mice as described above. Purified cells were activated with Dynabeads Mouse T-Activator CD3/CD28 (ThermoFisher)(1:1 cell:bead ratio) in the presence of recombinant human IL-2 (50ng/ml) (a gift from N. Rufer, DO UNIL) *in vitro* for 24 h before the addition of viral supernatant. Virus transduction was performed in the presence of polybrene (4mg/ml) (Sigma, TR-1003-G) during spin infection (1800rpm for 90min at 30°C) followed by overnight culture at 37°C. Transduced P14 cells (10^5) were injected i.v. into mice that had been infected with LCMV Arm one day before. Alternatively, P14 cells were kept in culture for 48 h and analyzed for the transduction efficiency.

Single cell RNA sequencing analysis

For scRNaseq, P14 cells were flow sorted from the spleen of naive *Tcf7*^{GFP} P14 reporter mice (CD62L^{+} CD8^{+}) (Naive), from B6 hosts (CD45.1/.2) transferred with *Tcf7*^{GFP} P14 cells at day 32 (d32) post LCMV Armstrong infection (Arm), from Vβ5 hosts (CD45.1) transferred with *Tcf7*^{GFP} P14 cells at d32 post LCMV clone13 infection (cl13), from B6 hosts (CD45.1/.2) transferred with d45 Arm *Tcf7*$^{GFP+}$ P14 cells at d42 post LCMV Arm infection (T_{CM} → Arm) or from B6 hosts (CD45.1/.2) transferred with d45 LCMV cl13 *Tcf7*$^{GFP+}$ P14 cells at d42 post LCMV Arm infection (T_{ML} → Arm). Each sample derived from a pool of 3 mice.

Cell lysis and RNA capture was performed according to the 10x Genomics protocol (Single Cell 3′ v3 chemistry). The cDNA libraries were generated according to the manufacturer's protocol (Illumina) and further sequenced (paired-end) with HiSeq2500 technology (Illumina) at the Gene Expression Core Facility (GECF) of the School of Life Sciences EPFL.

The raw sequencing reads were filtered, demultiplexed and aligned to the mouse genome (mm10) using the 10x Genomics Cell Ranger pipeline (version 3.0.1). The Cell Ranger pipeline was also used for dimensionality reduction and projection of the data with t-distributed stochastic neighbor embedding (t-SNE) (van der Maaten and Hinton, 2008). Subsequently, the raw count matrix was imported into R (v.4.0.3) and scRNaseq data was analyzed using the Seurat package (v.3.2.2) for R (Stuart et al., 2019). The raw count matrix was filtered to only retain cells that had between 800 and 3400 genes expressed (n = 26078) and to remove genes that were not expressed in any cell (n = 19775 expressed genes). The median number of mRNA detected per cell was n = 2070 genes for naive, n = 1841 for Arm, n = 1825 for cl13, n = 1762 for T_{CM} → Arm and n = 1599 for T_{ML} → Arm cells.

The filtered raw counts were log-normalized (to 10000 transcripts per cell) and scaled using the NormalizeData and ScaleData functions implemented in the Seurat package. The top 2000 most variable genes were selected to compute principal components. Cell clustering integrating all conditions was performed using the shared nearest neighbor (SNN) modularity optimization-based algorithm implemented in the FindNeighbors and FindClusters functions, with 15 principal components and a resolution parameter of 0.1. The clustering resulted in a total of 8 clusters, with clusters C1 to C6 encompassing 99.6% of all cells.

Genes differentially expressed between each cluster of cells and all other cells were determined using the FindAllMarkers function of the Seurat package, using the default parameters. Genes differentially expressed between specific pairs of clusters were determined using the FindMarkers function of the Seurat package, also using default parameters (i.e., Wilcoxon test and Bonferroni correction of *p-value*s (Table S2).

The gene expression profile of each cluster of cells was compared to gene signatures of two published bulk RNA sequencing datasets. Signatures were derived from naive P14 cells (T_N), from *Tcf7*$^{GFP+}$ and *Tcf7*$^{GFP-}$ P14 cells at d32 post LCMV Arm infection, which correspond to central memory (T_{CM}) and effector memory (T_{EM}) P14 cells, respectively (Pais Ferreira et al., 2020) and from *Tcf7*$^{GFP+}$ and *Tcf7*$^{GFP-}$ P14 cells at d32 post LCMV cl13 infection, which correspond to memory-like (T_{ML}) and exhausted (T_{EX}) P14 cells, respectively (GEO: GSE83978) (Utzschneider et al., 2016). Raw counts of the RNA sequencing data were filtered to only retain genes expressed at a minimum of 1 count per million (cpm) in at least 1 sample, normalization factors were calculated using the TMM method, and the data was converted to $\log_2$(cpm+1) using edgeR (v.3.32.0) (Robinson et al., 2010).

Correlation of the gene expression profile of each cluster of single cells to the expression profile of the cell types extracted from published RNA sequencing data were performed using the SingleR package (v.1.4.0) for R (Aran et al., 2019). The method implemented in the SingleR function initially selects genes that are differentially expressed between pairs of reference cell types by sorting the genes according to their log-fold change, then selecting the top $500*(2/3)^{\log2(N)}$ genes, where N is the number of different cell types included in the bulk RNaseq reference. Then, a Spearman correlation coefficient is calculated for each cluster of single cells against the expression of each reference cell type, using the union of the top genes selected. For the reference bulk RNA sequencing dataset we used, this resulted in 1440 genes being chosen to calculate correlation coefficients (see supplementary note 1 in Aran et al. [2019]). To associate *p-value*s to the Spearman correlation coefficients calculated by SingleR, we performed randomizations. Single cell cluster labels were randomized 10,000 times, and the nominal p value was estimated by calculating the proportion of random correlation scores that were higher than the real correlation score (p value = (number of higher random scores+1)/(number of randomizations +1)). The raw p values were subsequently ajusted using the BH procedure.

To determine whether or not differentially expressed genes were linked to pathways or gene sets, we performed gene set over-representation analysis using the enricher function of the clusterProfiler package (v.3.18.0), testing upregulated and downregulated genes separately, and adjusting p values using the Benjamini-Hochberg (BH) procedure (Benjamini and Hochberg, 1995). Lists of gene sets were obtained from the Molecular Signature Database (MSigDB) (Subramanian et al., 2005), namely the Hallmark gene sets (h.all.v7.1.symbols.gmt) (Liberzon et al., 2015) and the Pathway interaction database (PID) gene sets (c2.cp.pid.v7.2.symbols.gmt).

QUANTIFICATION AND STATISTICAL ANALYSIS

All bar and line graphs depict means ± SD. Statistical analyses were performed using Prism 7.0 or 8.0 (Graphpad Software). Unpaired t test (two-tailed, 95% confidence level) was used for the comparison of 2 datasets. Anova with Fisher test was used for > 2 comparison groups. *p-value*s < 0.05 were considered significant (*: $p < 0.05$; **: $p < 0.01$; ***: $p < 0.001$; ****: $p < 0.0001$); *p-value*s > 0.05 were considered non-significant (ns).